1521-0111/90/6/755–765$25.00
MOLECULAR PHARMACOLOGY

http://dx.doi.org/10.1124/mol.116.105049
Mol Pharmacol 90:755–765, December 2016

Molecular Basis for Inhibition of the Na^+/Citrate Transporter NaCT (SLC13A5) by Dicarboxylate Inhibitors[S]

Ana M. Pajor, Cesar A. de Oliveira, Kun Song, Kim Huard, Veerabahu Shanmugasundaram, and Derek M. Erion

University of California San Diego (A.M.P.), Skaggs School of Pharmacy and Pharmaceutical Sciences, La Jolla, California; Cardiovascular, Metabolic and Endocrine Disease Research Unit (K.S., K.H., D.M.E.), Pfizer Worldwide Research and Development, Cambridge, Massachusetts; Center of Chemistry Innovation and Excellence (C.A.O., V.S.), Pfizer Worldwide Research and Development, Groton, Connecticut

Received May 3, 2016; accepted September 26, 2016

ABSTRACT

The Na^+/citrate transporter, NaCT (SLC13A5), is a therapeutic target for metabolic diseases. Citrate is an important signaling molecule that regulates the activity of lipid- and glucose-metabolizing enzymes in cells. Previous studies identified two compounds, PF-06649298 (compound **2**) and PF-06678419 (compound **4**), that inhibit human NaCT with high affinity, and one of the compounds demonstrated specificity relative to other SLC13 family members. Here we use molecular modeling and site-directed mutagenesis of hNaCT followed by transport characterization and cell-surface biotinylation to examine the residues involved in inhibitor binding and transport. The results indicate that residues located near the putative citrate binding site, G228, V231, V232, and G409, affect both citrate transport and inhibition of citrate uptake by compounds **2** and **4**. V231 appears to distinguish between compounds **2** and **4** as inhibitors. Furthermore, residues located outside of the putative citrate binding site, Q77 and T86, may also play a role in NaCT inhibition by compounds **2** and **4**. Our results provide new insight into the mechanism of transport and inhibition in NaCT and the SLC13 family. These findings should provide a basis for future drug design of SLC13 inhibitors.

Introduction

The citric acid cycle intermediate citrate is a precursor to lipid and cholesterol biosynthesis and a nexus point between glucose and lipid. Intracellular citrate modulates the activity of key enzymes involved in fatty acid oxidation and glycolysis. Citrate products, such as malonyl CoA, have important signaling roles in regulation of energy expenditure (Ruderman et al., 1999). Circulating citrate concentrations affect feeding behavior and hepatic glucose metabolism, indicating that citrate can serve as an important energy signaling molecule (Gullans et al., 1988; Ruderman et al., 1999; Cesquini et al., 2008; Stoppa et al., 2008).

The Na^+-coupled di- and tricarboxylate transporters from the SLC13 family, NaDC1 (gene SLC13A2), NaDC3 (gene SLC13A3), and NaCT (gene SLC13A5), mediate the transport of citrate into cells and play important roles in determining cytosolic citrate concentrations (Pajor, 2014). The Na^+/dicarboxylate transporters, NaDC1 and NaDC3, transport monoprotonated citrate ($citrate^{2-}$). NaDC1 is predominantly found in kidney and small intestine, whereas NaDC3 has a broad tissue distribution in organs such as kidney, liver, brain, and placenta. In contrast, the Na^+-citrate transporter NaCT transports citrate in its trianionic form ($citrate^{3-}$) and, in humans, NaCT has a higher affinity for citrate than succinate (Inoue et al., 2002). NaCT is predominantly expressed in the liver, with lower expression in brain and testis (Inoue et al., 2002). NaCT expression in cells is correlated with increased lipid accumulation, through activation of the pregnane X receptor (Li et al., 2015).

The mammalian SLC13 transporters and their homologs have been shown to regulate metabolic processes. Inactivation of SLC13 homologs from flies [I'm not dead yet (INDY) gene] and worms results in lifespan extension through mechanisms related to caloric restriction (Rogina et al., 2000; Fei et al., 2004; Wang et al., 2009; Schwarz et al., 2015). Mutations in the human SLC13A3 gene that encodes NaDC3 are weakly associated with type 2 diabetes mellitus (T2DM) (Bento et al., 2008). Furthermore, deletion of the Na^+/citrate transporter (mNaCT, mIndy, *Slc13a5*) in mice results in increased energy expenditure, resistance to high-fat diet–induced metabolic abnormalities, and improvements in hepatic insulin responsiveness (Birkenfeld et al., 2011). Because of the metabolic changes associated with their inactivation, the transporters from the SLC13 family are emerging as new and important targets for treatment of T2DM and other metabolic disorders.

We recently reported a series of small, potent and selective dicarboxylates that are structurally related to citrate and capable of inhibiting NaCT-mediated cellular uptake of citrate in vitro and in vivo (Huard et al., 2015). Using a radiolabeled analog, we provided evidence that the dicarboxylates directly

dx.doi.org/10.1124/mol.116.105049.
[S] This article has supplemental material available at molpharm.aspetjournals.org.

ABBREVIATIONS: GAPDH, glyceraldehyde-3-phosphate dehydrogenase; HEK, human embryonic kidney; INDY, I'm not dead yet; h, human; m, mouse; SNT, Ser-Asn-Thr; TM, transmembrane helix; Vc, *Vibrio cholerae*.

and specifically interact with NaCT in a manner that is competitive with citrate, suggesting a common binding site within the transporter. Furthermore, we demonstrated that these dicarboxylates are recognized as substrates by NaCT, thus actively transported into the cells, resulting in higher intra- than extracellular concentration. One analog, PF-06649298 (compound **2**), selectively inhibited NaCT compared with NaDC1 and NaDC3, and a second analog, PF-06678419 (compound **4**), showed lower selectivity against NaDC1 and NaDC3 (Huard et al., 2015). Although there is no known high-resolution structure of any of the mammalian SLC13 transporters, an X-ray crystal structure of a bacterial homolog from *Vibrio cholerae* (Vc), VcINDY, was reported (Mancusso et al., 2012), which permits homology modeling (Schlessinger et al., 2014; Colas et al., 2015). VcINDY has a transport mechanism similar to that of the mammalian SLC13 family members, and the transporter cotransports dicarboxylates, such as succinate, together with two sodium ions (Mulligan et al., 2014). The structure of VcINDY is in an inward-facing conformation bound with a molecule of substrate and one sodium ion (Mancusso et al., 2012). In the present study, we prepared a homology model of the human NaCT on the basis of the VcINDY structure. Residues in human NaCT (hNaCT) that were predicted to be in the putative citrate binding site or at the extracellular surface providing access to the citrate binding site were evaluated by site-directed mutagenesis followed by functional characterization. The goals of these studies were to evaluate whether there is a common binding site for citrate and the dicarboxylate inhibitors, to identify residues that play a role in selectivity for NaCT versus NaDC1 and NaDC3, and to gain additional insight into the mechanism of inhibition by the dicarboxylate inhibitors. The results provide evidence for a set of residues in hNaCT involved in binding inhibitors and provide insight into inhibitor binding determinants of the SLC13 family.

Materials and Methods

Compounds. PF-06649298 (compound **2**) and PF-06678419 (compound **4**) were previously reported as high-affinity NaCT inhibitors that were identified because of their structural similarity with citrate (Fig. 1) (Huard et al., 2015). More specifically, both inhibitors display a 2-hydroxysuccinic acid motif that is common with citrate, and a functionalized 2-phenethyl substitution.

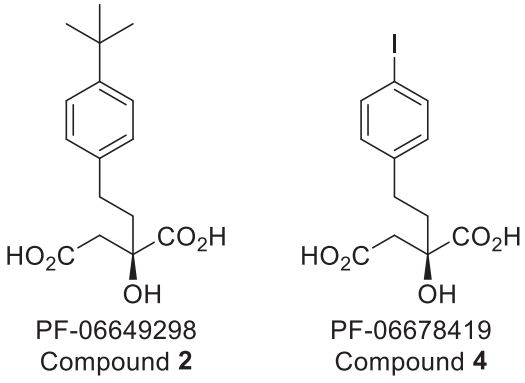

Fig. 1. Chemical structures of compounds used in this study. Compound **2** (PF-06649298), shown on the left, and compound **4** (PF-06678419), shown on the right, are described in more detail in our previous study (Huard et al., 2015).

Homology Modeling. A homology model of human NaCT (Uniprot ID Q86YT5) was built on the basis of the crystal structure of a bacterial sodium/dicarboxylate transporter, VcINDY (PDB ID: 4F35) (Mancusso et al., 2012). The VcINDY structure is in an inward-facing conformation with citrate and one of the two sodium ions bound (Mancusso et al., 2012). VcINDY and human NaCT share ~28% sequence identity. The sequence alignment (Fig. 2) and homology modeling (Fig. 3) were performed using the BioLuminate v. 1 software package (Schrödinger, LLC, New York, NY). The two units of the homodimer were built separately and then combined together. The sodium ions at Na1 sites of the two monomers were placed using the coordinates from the X-ray structure file. The conformations of missing loops were generated using Prime (Jacobson et al., 2004) in Maestro (Schrödinger, New York, NY). The final NaCT model (Fig. 3) was prepared and minimized following Protein Preparation Wizard workflow in Maestro (Sastry et al., 2013) .

Docking Studies. Docking protocols were carried out using the homology model of human NaCT described in the *Homology Modeling* section. The transporter was prepared by setting the receptor docking grid center around the citrate molecule, the cocrystallized ligand. The size of the inner and outer grid boxes was set to 10 Å in each direction. Structures of compounds **2** and **4** for docking studies were then generated with Maestro v. 9.2 (Schrödinger). The molecules were further refined using LigPrep v. 2.5 with the OPLS2005 force field (Schrödinger). Docking was carried out using XP precision with Glide v. 5.8 (Schrödinger) (Friesner et al., 2006).

Mutants and Cell Culture. Site-directed mutagenesis of human NaCT (SLC13A5) in pcDNA3.1 vector was done by Blue Sky Bioservices (Worcester, MA). Mutant and wild-type NaCT transporters were expressed in human embryonic kidney (HEK-293) cells (CRL-1573; American Type Culture Collection, Manassas, VA). The cells were cultured in Dulbecco's modified Eagle's medium supplemented with 25 mM HEPES, 2 mM glutamax, 1 mM Na-pyruvate, 0.1 mM nonessential amino acids, 10% heat-inactivated fetal calf serum, 100 IU/ml penicillin, and 100 μg/ml streptomycin at 37°C in 5% CO_2 (Pajor and Sun, 2013). The cells were plated on poly-D-lysine-coated 96-well plates (BD Biosciences, San Jose, CA) at 0.6×10^5 cells per well and transiently transfected using FuGene6 (Roche Applied Science, Indianapolis, IN) at a 3:1 ratio.

Transport Assays. Transport of 1,5-[^{14}C]citrate (112 mCi/mmol) (Moravek, La Brea, CA) was measured in the cells 48 hours after transfection, also as described (Pajor and Sun, 2013). The sodium transport buffer contained in mM: 140 NaCl, 2 KCl, 1 $MgCl_2$, 1 $CaCl_2$, 10 HEPES, pH adjusted to 7.4 with 1 M Tris. Choline buffer contained equimolar choline chloride in place of NaCl. For the assays, each well was washed twice with choline buffer and then incubated with 50 μl sodium buffer containing ~100 μM [^{14}C]-citrate (a combination of radioactive and nonradioactive citrate) for 30 minutes at room temperature. The uptake assays were stopped and the cells were washed four times with 250 μl choline buffer. Ultima Gold scintillation cocktail (Perkin Elmer, Waltham, MA) was added to each well and then the radioactivity in the plates was counted using a Wallac Microbeta plate scintillation counter (Perkin Elmer). For all experiments, backgrounds were corrected by subtracting the counts in vector-transfected cells from counts in SLC13 plasmid-transfected cells. The kinetic experiments were done with a constant amount of ^{14}C-citrate (approximately 20 μM) and increasing concentrations of nonradioactive citrate, up to 5 mM final concentration. For assays including inhibitors the cells were preincubated with inhibitor or dimethyl sulfoxide (DMSO) for 12 minutes before addition of a mixture of radioactive uptake solution containing inhibitor or DMSO (Pajor and Randolph, 2007). The final concentration of DMSO was 1%. The supply of compound **4** was limited and the IC_{50} was estimated from four concentrations rather than the full eight used for compound **2**. IC_{50} values were determined by fitting the data to a four-part logistic curve (SigmaPlot 10.0; Systat Software Inc., San Jose, CA).

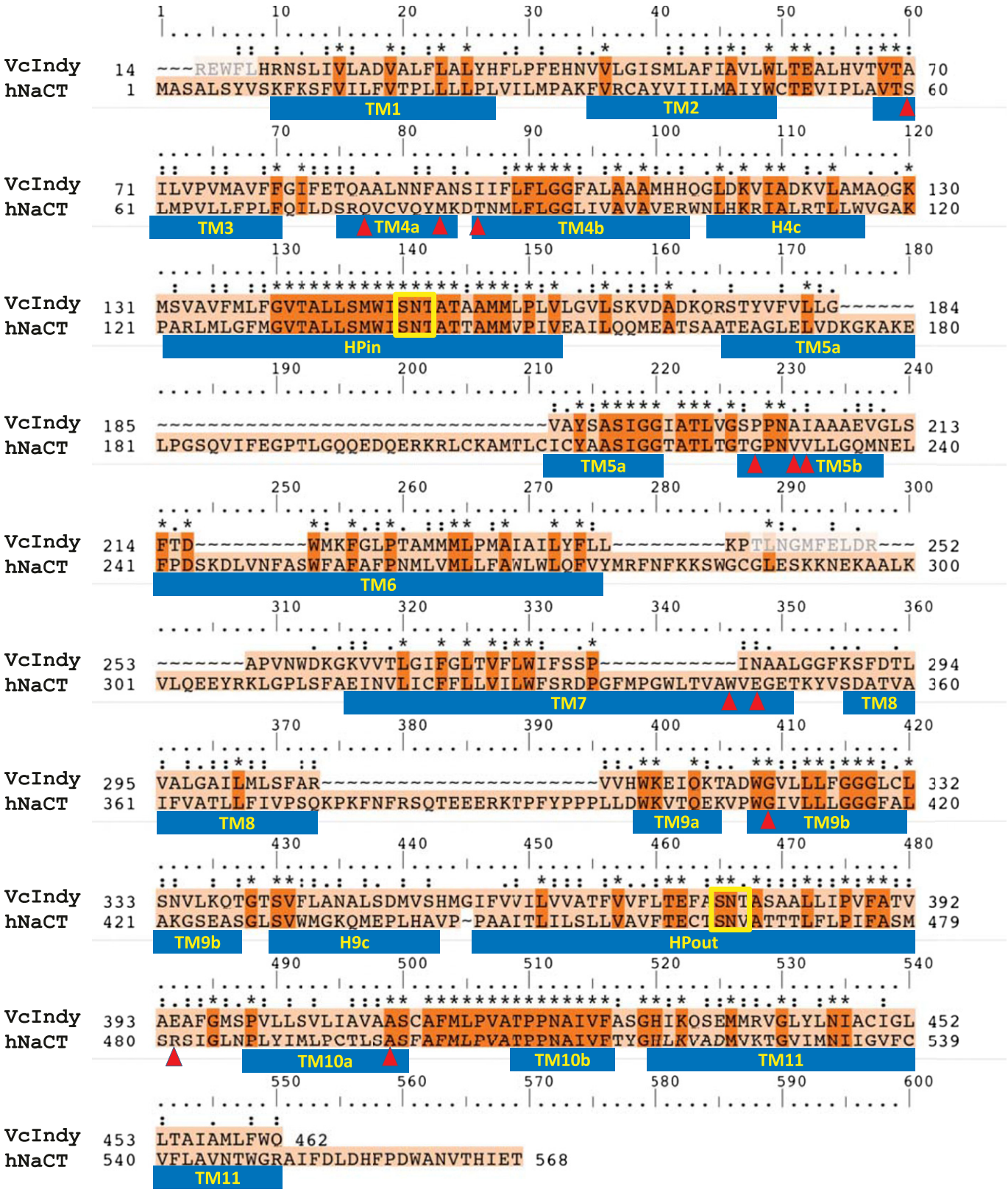

Fig. 2. Sequence alignment between hNaCT and VcINDY. The transmembrane helices (TM) and hairpin loop (HP_{in} and HP_{out}) motifs are indicated by blue bars under the sequences and the SNT motifs in HP_{in} and HP_{out} are outlined in yellow boxes. The residues mutated in this study are indicated using red triangles.

Anti-NaCT Antibodies. Polyclonal antibodies were raised in rabbits by Cambridge Research Biochemicals (Cambridge, UK), against NaCT peptide conjugated with keyhole limpet hemocyanin and bovine serum albumin. The peptide sequence was CGGKFNFRSQTEEERKTPFYP, corresponding to amino acids 376–392 of human NaCT. These antibodies were specific

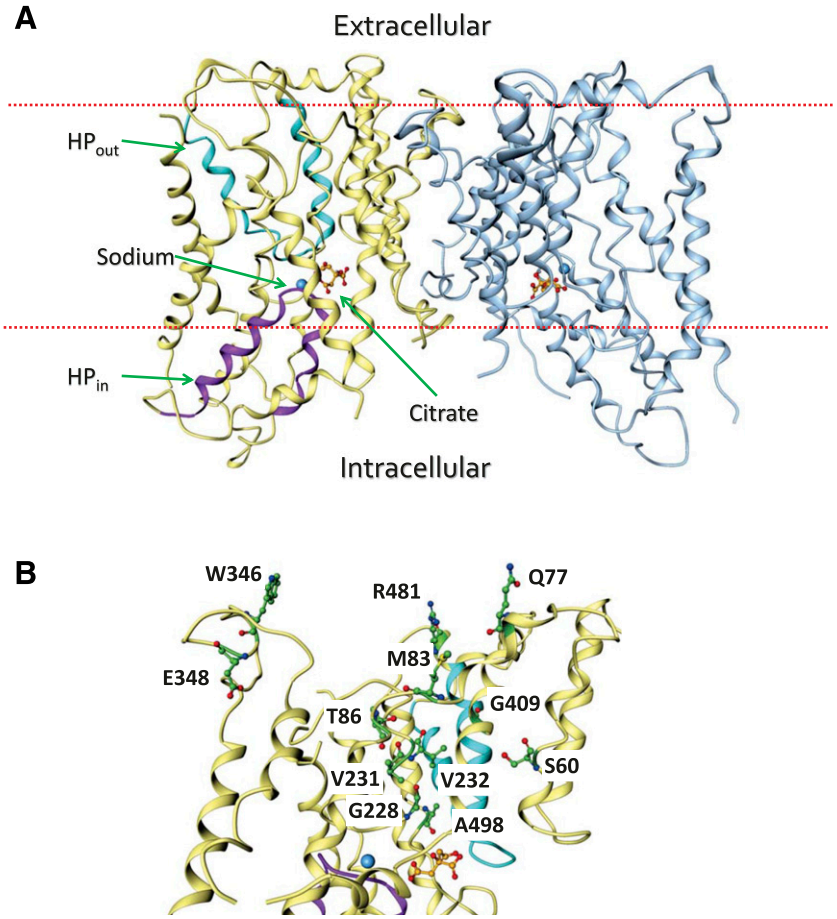

Fig. 3. Homology model of human NaCT. (A) The NaCT homodimer viewed from the side. The dotted line represents the plasma membrane. The hairpin loops are indicated by cyan (HP$_{out}$) and purple (HP$_{in}$) ribbons. The binding of the citrate molecule and one sodium ion (represented by a blue sphere) are shown on each monomer. (B) Side view of one NaCT monomer showing the positions of amino acids that were examined for mutagenesis.

for NaCT and did not recognize NaDC1 or NaDC3 (Supplemental Fig. 2A).

Western Blots. Cells were grown in six-well plates and lysed with RIPA buffer (bioWORLD, Dublin, OH) supplemented with protease inhibitors (10 μg/ml pepstatin, 10 μg/ml leupeptin, and 0.5 mM phenylmethanesulfonyl fluoride). Protein concentrations were measured with a DC Protein Assay kit (Bio-Rad Laboratories, Hercules, CA). Cell-surface proteins were identified using cell-surface biotinylation with Sulfo-NHS-LC-Biotin (ThermoFisher Scientific, Waltham, MA) for 30 minutes on ice, as described (Pajor and Randolph, 2005; Weerachayaphorn and Pajor, 2007). Three wells of a six-well plate were combined for each group. Human liver S9 fraction was purchased from Life Technologies/ThermoFisher Scientific. Samples were separated by Tricine SDS-PAGE, 7.5% (w/v), as described previously (Pajor and Sun, 1996). Equal amounts of protein were loaded per well, approximately 6 μg, made to a total volume of 20 μl. Chemiluminescent size standards were MagicMark XP (Invitrogen/ThermoFisher Scientific). The anti-NaCT primary antibody, applied at 1:750 dilution followed by secondary antibody at 1:10,000 dilution, was peroxidase-conjugated anti-rabbit IgG (Jackson Laboratories, Bar Harbor, ME). Protein loading was verified using duplicate blots probed with anti- glyceraldehyde-3-phosphate dehydrogenase (GAPDH) antibodies (1:10,000–15,000 dilution) (Ambion AM4300; ThermoFisher Scientific), followed by secondary antibody at 1:5000 dilution, peroxidase conjugated anti-mouse IgG (Jackson Laboratories). Detection was done with SuperSignal West Pico Chemiluminescent Substrate (ThermoFisher Scientific) and Image Station 4000R (Carestream Scientific, Rochester, NY).

Statistics. Duplicate or quadruplicate measurements were made for each data point. The experiments were repeated with at least three different batches of transfected cells from different passage numbers. Significant differences between groups were identified by one-way analysis of variance followed by Dunnett's multiple comparison test with $P < 0.05$.

Results

NaCT Model and Mutations. The hNaCT structure model was based on the X-ray crystal structure of the bacterial homolog VcINDY (Mancusso et al., 2012). In VcINDY, the opposing hairpin loops, HP$_{in}$ and HP$_{out}$, particularly the conserved Ser-Asn-Thr (SNT) motifs in those hairpin loops, are essential for sodium and carboxylate binding (Mancusso et al., 2012). The hairpin loops and SNT motifs are conserved in hNaCT (Fig. 2). The sequences of the SNT motifs and locations of the transmembrane helices are highlighted in the alignment.

The hNaCT model (Fig. 3A) shows the position of the 11-transmembrane helices (TM) and two opposing hairpin loops HP$_{in}$ and HP$_{out}$. This model is similar to previously reported homology models of human SLC13 family members, hNaDC1, hNaDC3, and hNaCT (Schlessinger et al., 2014; Colas et al., 2015). We docked the two test compounds, compounds **2** and **4**, in the putative citrate binding site of the hNaCT model. The poses clustered into two predominant binding conformations and top-ranked binding conformation was hypothesized as the binding mode and used for the mutagenesis studies (Supplemental Fig. 1). To identify

residues that could potentially play a role in selectivity within the SLC13 family, we selected residues that were different between NaCT and NaDC3 or NaDC1. The first group of residues for mutagenesis was located near the putative citrate binding site, within approximately 10 Å of the citrate molecule, because the functionalized 2-phenethyl group projects approximately 10 Å (Fig. 1). The mutated residues were G228, V231, V232, G409, and A498 (Figs. 2 and 3B). We also identified a second group of residues for mutagenesis that are predicted to be located on the extracellular surface of the protein and could potentially play a role in substrate accessibility to the binding site (Fig. 3B). The second group of residues for mutagenesis included S60, Q77, M83, T86, W346, E348, and R481. Most of the substitutions were with the equivalent residues from NaDC1 and NaDC3, and some additional substitutions were made at V231 and V232.

Inhibitors. We previously identified dicarboxylate compounds **2** and **4** as potent inhibitors of hNaCT (Huard et al., 2015). In the present study, the inhibitory effects of these compounds were verified with SLC13 family members in transiently transfected HEK-293 cells. Inhibition of citrate uptake in cells treated with compound **2** was specific for hNaCT, with no measurable inhibition of ^{14}C-citrate transport activity in the other SLC13 transporters, NaDC1 and NaDC3 (Fig. 4A). Compound **4** inhibited all three transporters at 100 μM concentration but inhibited NaCT to a greater degree than NaDC1 and NaDC3. There was no effect of these compounds on $^{35}SO_4$ transport by the Na^+/sulfate transporter, NaS1 (SLC13A1) (data not shown). Both compounds were effective inhibitors of NaCT, with IC_{50} values around 1 μM (compound **2**) and 1.7 μM (compound **4**) (Fig. 4B), which contrasts with the published values of 0.41 μM and 0.44 μM, respectively (Huard et al., 2015). The differences in IC_{50} values could be explained by the amount of overexpression of the transporter or the citrate concentration used in the uptake assay.

Citrate Transport Activity of Mutants. We prepared a total of 18 mutants of hNaCT using site-directed mutagenesis. The citrate transport activity of the mutants compared with the wild-type hNaCT is shown in Fig. 5A. Four of the mutants had no significant change in transport activity (Q77K, V231L, W346F, and E348P). Nine of the mutants had decreased activity that was between 24 and 62% of the wild-type (S60A, M83F, T86Q, T86S, T86Y, V231A, V231F, R481I, A498C). Five of the mutants (G228A, V232A, V232F, V232I, and G409N) had very low but detectable transport activity that was less than ~10% of the activity observed in the wild-type hNaCT transporter. We also examined citrate kinetic properties of the wild-type NaCT and seven of the mutants (Fig. 5B, Supplemental Table 1). The K_m for citrate in wild-type NaCT was approximately 300 μM (Fig. 5B, Supplemental Table 1). A previous study reported a K_m for citrate in hNaCT of 600 μM (Inoue et al., 2002), using a different cell line (HRPE rather than HEK-293). The differences in K_m values in SLC13 transporters can vary with membrane potential (Pajor et al., 1998). Consistent with the low transport activity observed with single concentrations of citrate, mutants G228A, V232A, and G409N had higher K_m values (1.2–4.3 mM) compared with the wild-type (Fig. 5B, Supplemental Table 1). The V231A mutant had a lower K_m than wild type, around 140 μM, and a lower V_{max}. The Q77K and T86Y mutants had similar citrate K_m values as the wild type but the V_{max} values were lower.

Western Blots. We used Western blotting to examine whether the changes in citrate transport activity in the NaCT mutants could be explained by changes in protein abundance. The anti-NaCT antibodies made for this study recognized multiple protein bands in NaCT-transfected cells, centered at ~35 kDa and 75 kDa (Fig. 6A and Supplemental Fig. 2A). Treatment of NaCT with the deglycosylating enzyme PNGaseF reduced the mass of the protein bands, indicating that NaCT has several glycosylated forms, similar to the related transporter NaDC1 (Pajor and Sun, 2010). The detergents used for

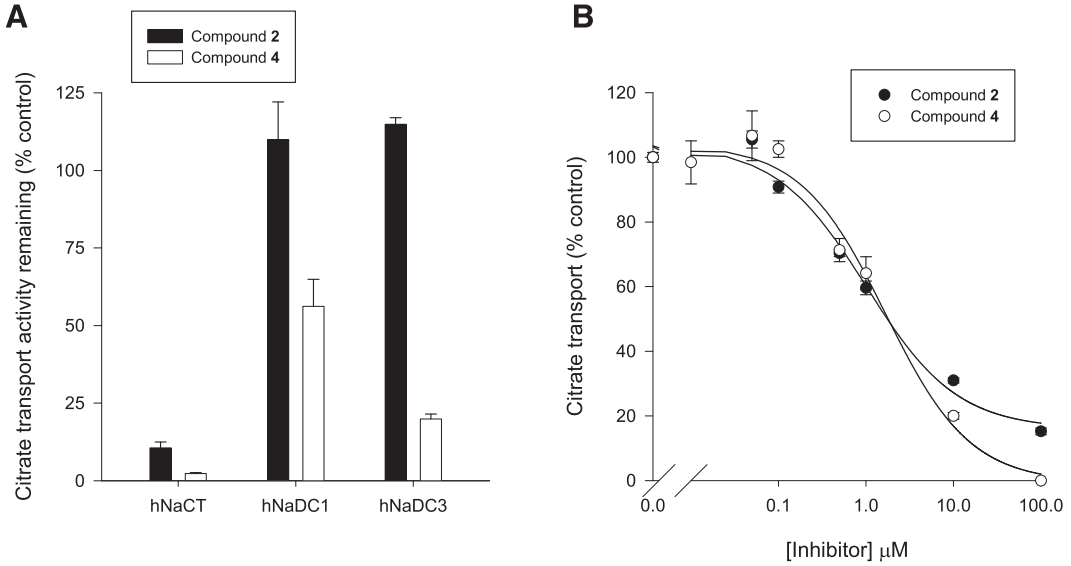

Fig. 4. Inhibition of citrate transport with compounds **2** and **4**. (A) Citrate transport activity in the presence of 100 μM inhibitor in HEK-293 cells expressing the human SLC13 family transporters: NaCT (SLC13A5), NaDC1 (SLC13A2), and NaDC3 (SLC13A3). Transport activity in the presence of inhibitor is shown as a percentage of the activity without inhibitor. Bars show means with S.E.M. (n = 3–4 NaCT) or range (n = 2 NaDC1, NaDC3). (B) Concentration dependence of inhibition by compounds **2** and **4**. HEK-293 cells expressing hNaCT were treated with increasing concentrations of inhibitor. The data were normalized to transport activity in the absence of inhibitor (DMSO control).

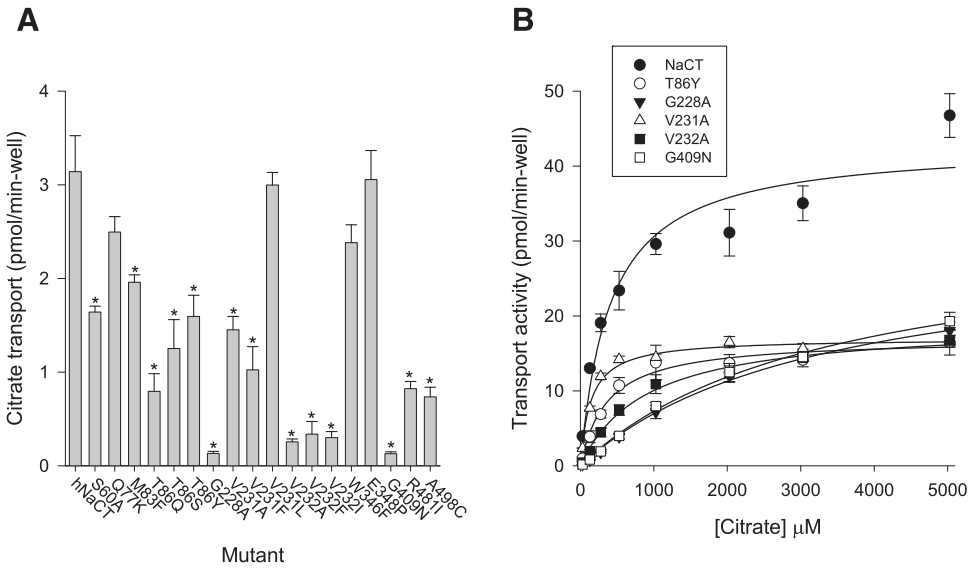

Fig. 5. Citrate transport activity in wild-type and mutant hNaCT. The transporters were expressed in HEK-293 cells. (A) Comparison of citrate transport activity in the mutants using 100 μM citrate. Bars are means ± S.E.M., n = 4–9 separate experiments. *Significantly different from wild-type NaCT, $P < 0.05$. (B) Citrate kinetics. Transport activity was measured at citrate concentrations between 20 μM and 5 mM. The data points show the mean ± S.E.M. of triplicate measurements from a single experiment.

the deglycosylation reaction could account for the change in mobility of the control sample (lane "–") (compare Supplemental Fig. 2, B and A). The NaCT-specific protein bands were not seen in control cells transfected with pcDNA vector alone (Fig. 6 and Supplemental Fig. 2A). The antibodies also recognized the native NaCT protein expressed in human liver homogenate S9 fraction (Supplemental Fig. 2C).

The expression analyses of NaCT wild-type and mutant protein abundance in whole-cell lysates were quantified using Western blots (Fig. 6A). The protein loading was verified by probing parallel blots with anti-GAPDH antibodies. The results show that all of the mutant proteins were expressed in the cells and there were no large differences in total protein abundance (Fig. 6A). We also examined cell-surface protein expression in some of the mutant transporters labeled with membrane impermeant Sulfo-NHS-LC-biotin (Fig. 6B). The signals from the cell-surface biotinylation experiments were not as strong as from the whole-cell lysates, and there was considerable variation in signal intensity between different experiments (Fig. 6B and Supplemental Fig. 4). The cell-surface expression of G228A, T86Y, V231L, and G409N was higher than that of the wild-type NaCT, whereas the cell-surface expression of Q77K, V231A, V232A, R481I, and A498C was consistently lower than that of the wild-type.

Sodium Activation of Citrate Transport. NaCT is a sodium-coupled di- and tricarboxylate transporter that couples four sodium ions to the transport of each substrate molecule (Inoue et al., 2004). This coupled transport appears cooperative, with a sigmoid relationship between sodium concentration and citrate transport activity (Inoue et al., 2003). The hNaCT model has a putative Na1 Na^+ binding site located in close proximity to the citrate binding site (Fig. 3).

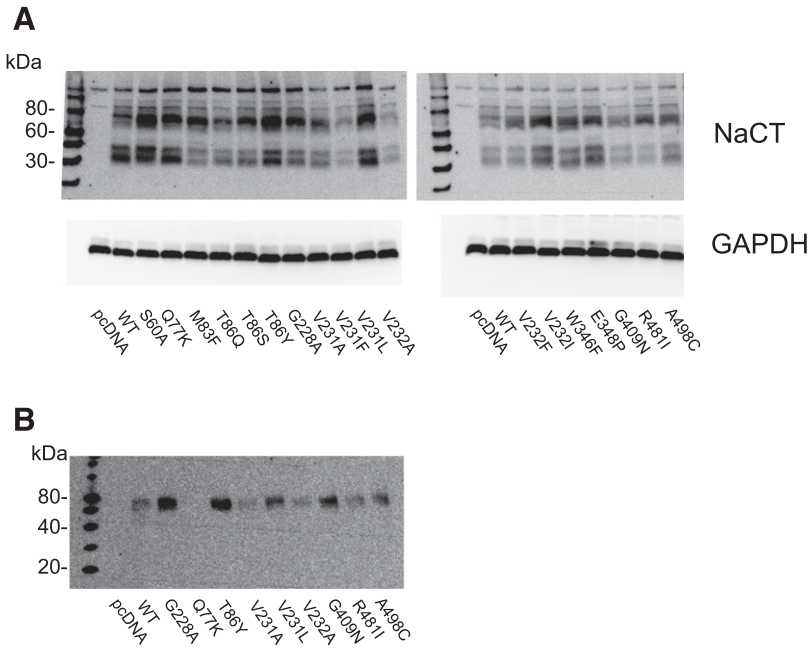

Fig. 6. (A) Western blots of total protein lysates of HEK-293 cells expressing hNaCT mutants. Each lane was loaded with ~6 μg of protein. Sizes of molecular mass standards [MagicMark XP (ThermoFisher Scientific)] are shown at the left. The proteins were detected with anti-NaCT antibody at 1:750 dilution (upper blot), and protein loading was verified by a duplicate blot probed with anti-GAPDH antibody (lower blot). (B) Cell-surface biotinylations of wild-type and mutant NaCT. HEK-293 cells expressing the transporters were treated with the membrane impermeant reagent Sulfo-NHS-LC-biotin as described in *Materials and Methods*. The Western blots were probed with anti-NaCT antibody, as in (A).

Therefore, we examined whether there were changes in the handling of sodium by NaCT mutants. Sodium activation kinetics by human NaCT typically do not show saturation at the highest concentration of sodium (Inoue et al., 2002, and our own unpublished observations), making it difficult to accurately measure $K_{0.5}$ for sodium. Therefore, we estimated changes in apparent sodium affinity in the mutants by measuring citrate transport activity at two sodium concentrations, an approach used for hNaDC3 in a previous study (Schlessinger et al., 2014). The wild-type NaCT had approximately 25% transport activity at 70 mM versus 140 mM sodium, and there were no significant differences in any of the mutants (Fig. 7). These results indicate that the mutations affect substrate transport without changing the apparent sodium affinity in this concentration range.

Citrate Transport Inhibition by Compounds 2 and 4. The citrate transport activity of the mutants was measured in the presence and absence of the two inhibitors (Figs. 8A and 9A). Compound **2** is a selective NaCT inhibitor, whereas compound **4** inhibits NaCT, NaDC1, and NaDC3 at concentrations greater than 30 μM (Fig. 4 and Huard et al., 2015). Since both compounds are structurally similar, we were interested in understanding the differential activity profiles in mutant NaCT protein in order to potentially explain the selectivity. As shown in Figs. 8A and 9A, some of the mutations negatively affected inhibition by both compounds **2** and **4**, and the observed inhibition of citrate transport was decreased for mutants G228A, V232A, V232I, G409N, and R481I compared with wild type. Some of the mutations primarily affected inhibition by compound **2** (V231F,L and A498C), indicating that these residues may determine differential activity and selectivity profiles in binding between the two compounds.

We also examined the concentration dependence of inhibition by compounds **2** and **4** in the wild type and seven mutants (Figs. 8B and 9B and Supplemental Tables 2 and 3). The IC_{50} for compound **2** in wild-type NaCT was approximately 1 μM, and for compound **4**, the IC_{50} was 1.4 μM, similar to the experiment shown in Fig. 4B. The IC_{50} values for the T86Y and V231A mutants were significantly lower with both compounds compared with the wild type, whereas the Q77K mutant was significantly lower with compound **4** (Supplemental Table 2). The inhibition curve for V231L with compound **2** was shifted to the right (Fig. 8B), indicating a decrease in affinity, although it was not possible to determine the IC_{50} value accurately. V231L had a significant decrease in IC_{50} for compound **4** (Supplemental Table 2). The V232A mutant appeared to have lower affinity for compound **2**, with IC_{50} values of 30 and 24 μM. Both G228A and G409N were insensitive to inhibition by compounds **2** and **4**. The curves could not be fitted accurately, probably because of incomplete inhibition at the highest concentrations tested. Supplemental Table 3 shows that the IC_{50} values for compound **2** in G228A and G409N are at least 250 μM because both mutants had approximately 50–60% citrate transport activity remaining at that concentration. Similarly, both mutants have IC_{50} values for citrate uptake by compound **4** of at least 25 μM.

Proposed Binding Modes of High-Affinity Inhibitors. We used the homology model to propose binding modes of compounds **2** and **4** with hNaCT. Figure 10, A and B, displays the respective docked poses of compounds **2** and **4** in the putative binding site and location of NaCT residues mutated in this study (Gly228, Gly409, Ala498, Val231, and Val232). Both compounds are proposed to adopt a binding mode in which the hydroxysuccininc acid motif mimics the position of citrate in the published crystal structure of VcINDY. In this binding mode, the aryl substituent (*t*-Bu and iodo for compounds **2** and **4**, respectively) is placed deep in the binding site. Figure 11 depicts a close-in view of compound **2** modeled in the putative binding site. Of the residues mutated in this study, Val231 and Val232 interact with compound **2** by making hydrophobic contacts with the *t*-butyl phenyl group. The succinic acid moiety of compound **2** forms hydrogen-bonding interactions with Asn141 from the SNT motif that binds citrate, and interacts with sodium through electrostatic interactions. A surface representation of the putative binding site indicates that compound **2** fits the space and the t-butyl group is oriented toward the extracellular surface of the

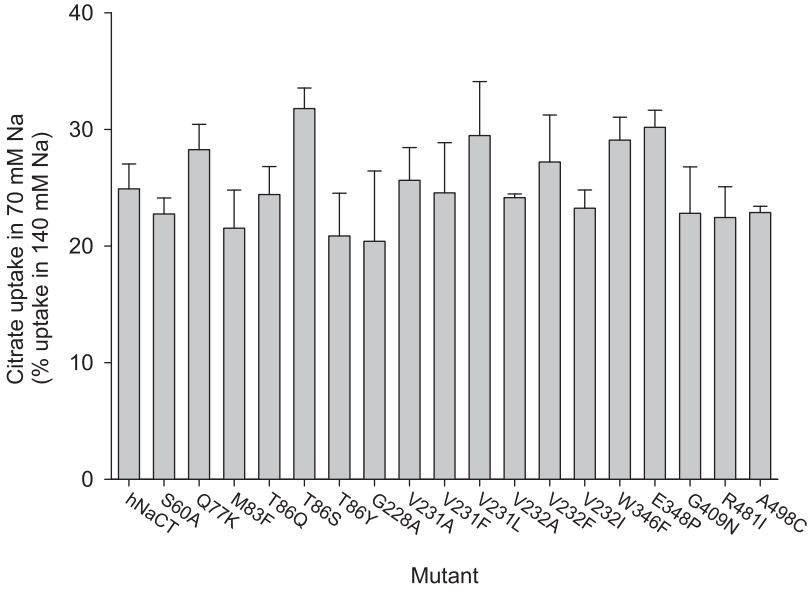

Fig. 7. Unaffected sodium handling by NaCT mutants. Citrate transport activity was measured in transport buffer containing 70 mM Na^+ plus 70 mM choline and is shown as a percentage of the transport activity in 140 mM Na^+. There were no significant differences in the mutants compared with wild-type NaCT. Bars are means ± S.E.M., n = 3–4 independent experiments (mutants) or 6 wild-type.

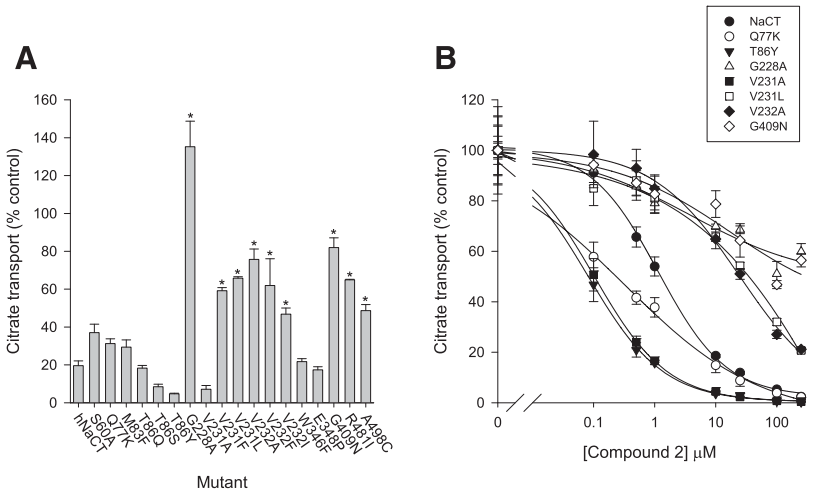

Fig. 8. Sensitivity to inhibition by compound **2**. Citrate transport activity was measured in HEK-293 cells expressing hNaCT wild type and mutants. (A) The activity was measured in the presence of 10 μM compound **2** and expressed as a percentage of the transport activity without compound (control, DMSO only). Bars are means ± S.E.M., n = 3–5 mutants or 8 wild-type. *Significantly different from wild-type NaCT, $P < 0.05$. (B) Concentration dependence of inhibition by compound **2**. Transport of ~20 μM ^{14}C-citrate was measured at increasing concentrations of compound **2** and activity was expressed as a percentage of the transport activity without compound (control, DMSO only). The data points represent triplicate measurements (mean ± S.E.M.) from a single experiment.

protein, whereas the diacid moiety is pointing toward the intracellular compartment.

Discussion

The citric acid cycle intermediate, citrate, is an important signaling molecule that regulates the activity of lipid- and glucose-metabolizing enzymes. The Na^+/citrate transporter NaCT, from the SLC13 family, mediates citrate transport into cells from the extracellular fluid and is most abundant in the liver (Inoue et al., 2002; Li et al., 2016). Deletion of this transporter in mice produces substantial metabolic changes and protection against the deleterious effects of a high-fat diet (Birkenfeld et al., 2011). Our recent study has identified two potent inhibitors of human NaCT (compounds **2** and **4**) that block citrate uptake in vitro and in vivo (Huard et al., 2015). In the present study we combine modeling and experimental testing to identify specific residues in NaCT that are important for inhibitor binding and selectivity. The main findings presented are that residues near the putative citrate binding site as well as residues outside of the binding site participate in inhibition of citrate transport by compounds **2** and **4**. These findings provide new insight into the specificity determinants of NaCT and the other members of the SLC13 family.

A key step in understanding the mechanism of transport of NaCT and its involvement in metabolism is the design of effective, potent, and specific inhibitors. In this study we examined residues in NaCT that potentially interact with two test inhibitors, compounds **2** and **4**, both derivatives of citrate with functionalized phenethyl substitutions at the second carbon (Huard et al., 2015). Compound **2** is both a substrate and inhibitor of NaCT that binds to NaCT in a stereosensitive manner (Huard et al., 2015). By blocking citrate uptake in liver, compound **2** produced a reduction in the conversion of extracellular citrate into tricarboxylic acid cycle intermediates, which resulted in reductions of plasma glucose concentrations in high-fat fed mice treated with compound **2** (Huard et al., 2015). In the present study we verified that NaCT inhibition by compounds **2** and **4** is potent, with micromolar IC_{50} values, compared with the citrate K_m value of around 300 μM. Compound **2** is completely selective for NaCT, whereas compound **4** inhibits NaCT, NaDC1, and NaDC3.

We used molecular modeling and site-directed mutagenesis of hNaCT to identify common binding sites between the inhibitors and citrate and to understand the selectivity observed with compound **2**. Residues were selected from two regions, either within 10Å of the citrate binding site or outside the binding site, near the extracellular surface of the transporter. The extracellular surface residues could determine access to the substrate binding site or could determine flexibility during the large conformational changes observed during transport (Mulligan et al., 2016). Overall, we found

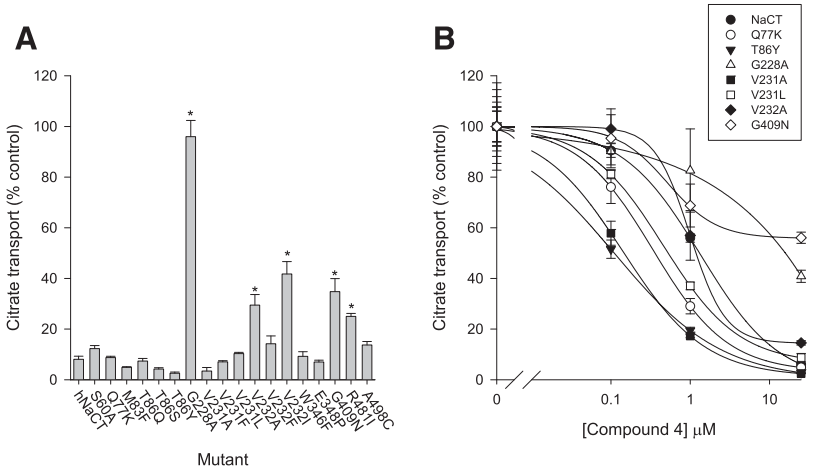

Fig. 9. Sensitivity of inhibition by compound **4**. (A) Citrate transport activity in wild-type and mutant NaCT measured with 10 μM compound **4**. Bars are means ± S.E.M., n = 3–5 mutants or 8 wild-type. *Significantly different from wild-type NaCT, $P < 0.05$. (B) Concentration dependence of inhibition by compound **4** (see legend, Fig. 8).

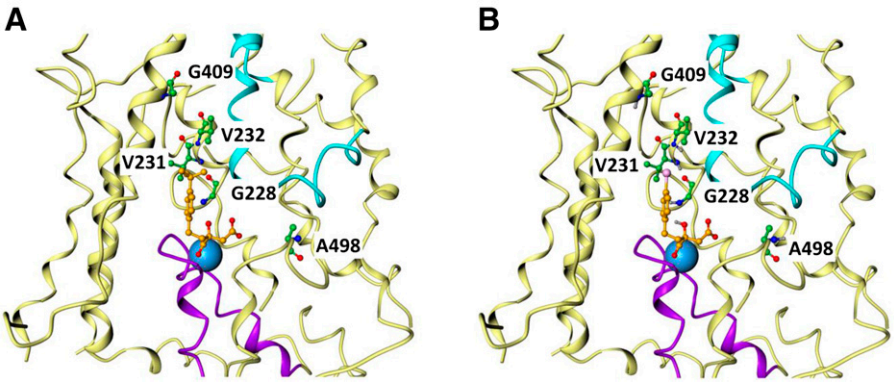

Fig. 10. Docking poses of compounds **2** (A) and **4** (B) in NaCT. The compound structures are shown as orange sticks. The Na^+ ion at the Na1 site is shown as a blue sphere. The positions of some of the residues mutated in this study are indicated (A498, G228, V231, V232, and G409).

that mutations close to the predicted citrate binding site were deleterious to citrate transport and also affected inhibitor binding. The G228A mutation in TM5b reduced affinity for citrate and for both compounds, despite reasonable protein expression on the cell surface. This result is in agreement with a model (Fig. 10) in which G228 makes direct contact with citrate and both compounds. The G409N mutation located in TM9b, confirmed to be on the plasma membrane, also had decreased affinity for citrate and both inhibitors. Both mutations involved increasing side-chain volume, from a glycine residue to an alanine or asparagine. Therefore, the mutations may produce a steric or size effect that affects access of the compounds to the putative binding site. Val232 is approximately midway along TM5a (Fig. 10). This residue is also important for NaCT's function because all of the mutations tested at this position decreased both citrate transport and inhibitory activity of compounds **2** and **4**. The V232A mutant had an increased K_m for citrate, and a decreased protein expression, reflected in a decreased V_{max} for citrate. The results with Val232 are consistent with the model (Fig. 10), in which Val232 is located in close proximity to the aryl substituent of the inhibitors and replacement of the valine by bulkier side chains would likely prohibit binding of compounds **2** and **4**. The adjacent residue, Val231, appears to distinguish between compounds **2** and **4**. When replaced by Leu, the residue found at the equivalent position in NaDC1 and NaDC3, the citrate kinetics and protein expression are similar to wild type. However, there is less inhibition of V231L by compound **2**, indicating a decrease in affinity, yet the apparent affinity for compound **4** is increased, producing an inhibitor sensitivity profile similar to NaDC1 and NaDC3. In the V231A mutant, however, the affinity for citrate and both compounds increased, confirming a role for Val231 in citrate binding. According to the proposed binding mode (Fig. 11 and Supplemental Fig. 1), Val231 is located in the citrate binding site, making direct interactions with the *t*-butyl group of compound **2**.

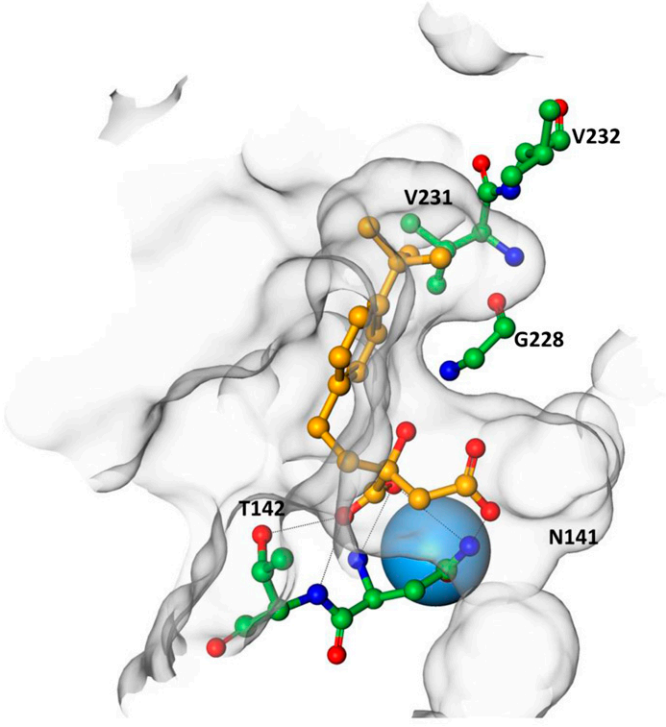

Fig. 11. Close-up view of compound **2** binding in NaCT. Compound **2** is shown as orange sticks. The blue sphere represents the Na^+ ion at the Na1 binding site. The putative binding site formed by surrounding residues is represented as a transparent surface.

Another key finding from our study is that residues in hNaCT that are outside of the substrate binding site also influence transport and inhibition by compounds **2** and **4**. The second group of NaCT mutants created is located at or near the outer surface of the protein, particularly TM5 and HP_{out}. These extracellular residues are important for both transport and inhibition, suggesting that these residues play a role in substrate access to the citrate binding site when the transporter is in an outward facing conformation. Alternatively, these residues may be needed for large conformational changes required for the transport of substrate by NaCT. The Q77K and T86Y mutants are located outside of the substrate binding site in TM4 (Fig. 3). These mutants do not affect citrate K_m but they appear to decrease the IC_{50} for one or both compounds. The mechanism of this is not yet known. This part of the protein in other SLC13 transporters changes accessibility to the outside of the cell during transport, either because the residue is moving during binding or transport or because other residues are occluding it (Weerachayaphorn and Pajor, 2007; Joshi and Pajor, 2009). The W346F and E348P mutants, located in the extracellular loop between helices M7 and M8 (Fig. 3), do not appear to participate in transport or inhibition of citrate, consistent with the potential role of these helices as a fixed scaffold structure (Mancusso et al., 2012; Mulligan et al., 2016).

None of the binding site mutants had an effect on sodium handling by NaCT, indicating that they do not produce significant structural and functional disruption despite their

proximity to the sodium binding sites in the proposed structure. In our model, the sodium ion at Na1 is thought to be coordinated partially by one of the carboxyl groups of the substrate. Aligned with this, Thevenon et al. (2014) recently identified variants of NaCT that cause autosomal-recessive epileptic encephalopathy. Two of the three residues specifically associated with the phenotype in their study (Gly219, Thr227, and Leu488) are located directly in the proposed sodium binding site in our model. This is consistent with their hypothesis that these mutations affect the ability of NaCT to bind sodium. By comparison, mutations in Na^+ binding sites of NaDC3 (SLC13A3) produced a large decrease in affinity for sodium (Schlessinger et al., 2014). The VcINDY crystal structure provides information on the location of two sodium binding sites, called Na1 and Na2 (Mancusso et al., 2012). NaCT couples four sodium ions to the transport of citrate (Inoue et al., 2004), but there is no information yet on the positions of Na3 and Na4. A recent model of human NaPi-IIa, which is believed to have the same fold as VcINDY, identified three sodium binding sites all in close proximity (Fenollar-Ferrer et al, 2015).

The specific mechanism of inhibition by compounds **2** and **4** is not yet fully understood. Our previous study showed that compound **2** is a transported substrate of hNaCT (Huard et al., 2015). Furthermore, we found evidence that compound **2** can inhibit NaCT from the intracellular portion of the cell (Huard et al., 2015). Citrate uptake was inhibited when a permeable prodrug was used to partition compound **2** into the cells, suggesting that inhibition of the transporter can occur from the intracellular compartment. Our results from the present study are consistent with both compounds sharing a binding site with citrate but with some of the selectivity determinants located outside the citrate binding site. In this model, competitive inhibition can occur by binding of the inhibitor from the intracellular compartment to the citrate binding site when the transporter is in an inward-facing conformation. Although compound **2** is transported into the cell via hNaCT, it is possible that the affinity for compound **2** as a competitive inhibitor is greatest in the inward-facing conformation. More detailed studies are being conducted to better understand the mechanism of action, and the complex kinetics of inhibition will be reported separately. Altogether, the results presented here are consistent with a model in which extracellular residues play a role in substrate recruitment and accessibility to the citrate binding site when NaCT is in an outward-facing conformation, whereas inhibition depends on the intracellular concentration of the inhibitor. No residues located on the intracellular face of the protein were investigated in this work. Our results do not preclude that an allosteric site may exist to allow binding of the compounds, thus preventing movement of the protein and therefore transport of substrates. In this scenario, the residues mutated in this study could influence the potency of compounds **2** and **4** by altering their transport and effectively impacting the intracellular concentrations of inhibitors. It should be noted that the interpretation of the results from this study is limited since modeling and docking could only be performed in the inward-facing conformation of NaCT. More structures, and in particular structures with the inhibitors bound, are needed to better understand this system.

In conclusion, this study demonstrates that key residues in two distinct domains of NaCT provide specificity determinants for inhibition. First, residues located within 10 Å of the citrate binding site are important for both citrate and inhibitor binding. In particular, Val231 appears to distinguish between compound **2** and **4**. Second, residues located outside the citrate binding sites are also important for inhibition by these two compounds, possibly by allowing access to the binding site. The structural model of hNaCT provides a framework for understanding the mechanism of transport and inhibition of this protein. These findings should provide a basis for future drug design of SLC13 inhibitors.

Acknowledgments

The authors thank Nina Sun and Diana Rozenshteyn for technical assistance with the cell culture experiments.

Authorship Contributions

Participated in research design: Pajor, de Oliveira, Song, Huard, Shanmugasundaram, Erion.

Conducted experiments: Pajor, de Oliveira, Song.

Performed data analysis: Pajor, de Oliveira, Song, Huard, Shanmugasundaram, Erion.

Wrote or contributed to the writing of the manuscript: Pajor, de Oliveira, Song, Huard, Sanmugasundaram, Erion.

References

Bento JL, Palmer ND, Zhong M, Roh B, Lewis JP, Wing MR, Pandya H, Freedman BI, Langefeld CD, Rich SS, et al. (2008) Heterogeneity in gene loci associated with type 2 diabetes on human chromosome 20q13.1. *Genomics* **92**:226–234.

Birkenfeld AL, Lee HY, Guebre-Egziabher F, Alves TC, Jurczak MJ, Jornayvaz FR, Zhang D, Hsiao JJ, Martin-Montalvo A, Fischer-Rosinsky A, et al. (2011) Deletion of the mammalian INDY homolog mimics aspects of dietary restriction and protects against adiposity and insulin resistance in mice. *Cell Metab* **14**:184–195.

Cesquini M, Stoppa GR, Prada PO, Torsoni AS, Romanatto T, Souza A, Saad MJ, Velloso LA, and Torsoni MA (2008) Citrate diminishes hypothalamic acetyl-CoA carboxylase phosphorylation and modulates satiety signals and hepatic mechanisms involved in glucose homeostasis in rats. *Life Sci* **82**:1262–1271.

Colas C, Pajor AM, and Schlessinger A (2015) Structure-based identification of inhibitors for the SLC13 family of Na^+/dicarboxylate cotransporters. *Biochemistry* **54**:4900–4908.

Fei YJ, Liu JC, Inoue K, Zhuang L, Miyake K, Miyauchi S, and Ganapathy V (2004) Relevance of NAC-2, an Na+-coupled citrate transporter, to life span, body size and fat content in Caenorhabditis elegans. *Biochem J* **379**:191–198.

Fenollar-Ferrer C, Forster IC, Patti M, Knoepfel T, Werner A, and Forrest LR (2015) Identification of the First Sodium Binding Site of the Phosphate Cotransporter NaPi-IIa (SLC34A1). *Biophys J* **108**:2465–2480.

Friesner RA, Murphy RB, Repasky MP, Frye LL, Greenwood JR, Halgren TA, Sanschagrin PC, and Mainz DT (2006) Extra precision glide: docking and scoring incorporating a model of hydrophobic enclosure for protein-ligand complexes. *J Med Chem* **49**:6177–6196.

Gullans SR, Kone BC, Avison MJ, and Giebisch G (1988) Succinate alters respiration, membrane potential, and intracellular K^+ in proximal tubule. *Am J Physiol* **255**: F1170–F1177.

Huard K, Brown J, Jones JC, Cabral S, Futatsugi K, Gorgoglione M, Lanba A, Vera NB, Zhu Y, Yan Q, et al. (2015) Discovery and characterization of novel inhibitors of the sodium-coupled citrate transporter (NaCT or SLC13A5). *Sci Rep* **5**:17391.

Inoue K, Fei YJ, Zhuang L, Gopal E, Miyauchi S, and Ganapathy V (2004) Functional features and genomic organization of mouse NaCT, a sodium-coupled transporter for tricarboxylic acid cycle intermediates. *Biochem J* **378**:949–957.

Inoue K, Zhuang L, and Ganapathy V (2002) Human Na^+ -coupled citrate transporter: primary structure, genomic organization, and transport function. *Biochem Biophys Res Commun* **299**:465–471.

Inoue K, Zhuang L, Maddox DM, Smith SB, and Ganapathy V (2003) Human sodium-coupled citrate transporter, the orthologue of Drosophila *Indy*, as a novel target for lithium action. *Biochem J* **374**:21–26.

Jacobson MP, Pincus DL, Rapp CS, Day TJ, Honig B, Shaw DE, and Friesner RA (2004) A hierarchical approach to all-atom protein loop prediction. *Proteins* **55**: 351–367.

Joshi AD and Pajor AM (2009) Identification of conformationally sensitive amino acids in the $Na^{(+)}$/dicarboxylate symporter (SdcS). *Biochemistry* **48**:3017–3024.

Li L, Li H, Garzel B, Yang H, Sueyoshi T, Li Q, Shu Y, Zhang J, Hu B, Heyward S, et al. (2015) SLC13A5 is a novel transcriptional target of the pregnane X receptor and sensitizes drug-induced steatosis in human liver. *Mol Pharmacol* **87**:674–682.

Li Z, Erion DM, and Maurer TS (2016) Model-based assessment of plasma citrate flux into the liver: Implications for NaCT as a therapeutic target. *CPT Pharmacometrics Syst Pharmacol* **5**:132–139.

Mancusso R, Gregorio GG, Liu Q, and Wang DN (2012) Structure and mechanism of a bacterial sodium-dependent dicarboxylate transporter. *Nature* **491**:622–626.

Mulligan C, Fenollar-Ferrer C, Fitzgerald GA, Vergara-Jaque A, Kaufmann D, Li Y, Forrest LR, and Mindell JA (2016) The bacterial dicarboxylate transporter VcINDY uses a two-domain elevator-type mechanism. *Nat Struct Mol Biol* **23**: 256–263.

Mulligan C, Fitzgerald GA, Wang DN, and Mindell JA (2014) Functional characterization of a Na^+-dependent dicarboxylate transporter from Vibrio cholerae. *J Gen Physiol* **143**:745–759.
Pajor AM (2014) Sodium-coupled dicarboxylate and citrate transporters from the SLC13 family. *Pflugers Arch* **466**:119–130.
Pajor AM, Hirayama BA, and Loo DDF (1998) Sodium and lithium interactions with the Na^+/dicarboxylate cotransporter. *J Biol Chem* **273**:18923–18929.
Pajor AM and Randolph KM (2005) Conformationally sensitive residues in extracellular loop 5 of the Na^+/dicarboxylate co-transporter. *J Biol Chem* **280**:18728–18735.
Pajor AM and Randolph KM (2007) Inhibition of the Na^+/dicarboxylate cotransporter by anthranilic acid derivatives. *Mol Pharmacol* **72**:1330–1336.
Pajor AM and Sun N (1996) Characterization of the rabbit renal Na^+-dicarboxylate cotransporter using antifusion protein antibodies. *Am J Physiol* **271**:C1808–C1816.
Pajor AM and Sun NN (2010) Single nucleotide polymorphisms in the human Na^+-dicarboxylate cotransporter affect transport activity and protein expression. *Am J Physiol Renal Physiol* **299**:F704–F711.
Pajor AM and Sun NN (2013) Nonsteroidal anti-inflammatory drugs and other anthranilic acids inhibit the Na^+/dicarboxylate symporter from *Staphylococcus aureus*. *Biochemistry* **52**:2924–2932.
Rogina B, Reenan RA, Nilsen SP, and Helfand SL (2000) Extended life-span conferred by cotransporter gene mutations in Drosophila. *Science* **290**:2137–2140.
Ruderman NB, Saha AK, Vavvas D, and Witters LA (1999) Malonyl-CoA, fuel sensing, and insulin resistance. *Am J Physiol* **276**:E1–E18.
Sastry GM, Adzhigirey M, Day T, Annabhimoju R, and Sherman W (2013) Protein and ligand preparation: parameters, protocols, and influence on virtual screening enrichments. *J Comput Aided Mol Des* **27**:221–234.
Schlessinger A, Sun NN, Colas C, and Pajor AM (2014) Determinants of substrate and cation transport in the human Na^+/dicarboxylate cotransporter NaDC3. *J Biol Chem* **289**:16998–17008.
Schwarz F, Karadeniz Z, Fischer-Rosinsky A, Willmes DM, Spranger J, and Birkenfeld AL (2015) Knockdown of Indy/CeNac2 extends Caenorhabditis elegans life span by inducing AMPK/aak-2. *Aging (Albany, NY)* **7**:553–567.
Stoppa GR, Cesquini M, Roman EA, Prada PO, Torsoni AS, Romanatto T, Saad MJ, Velloso LA, and Torsoni MA (2008) Intracerebroventricular injection of citrate inhibits hypothalamic AMPK and modulates feeding behavior and peripheral insulin signaling. *J Endocrinol* **198**:157–168.
Thevenon J, Milh M, Feillet F, St-Onge J, Duffourd Y, Jugé C, Roubertie A, Héron D, Mignot C, Raffo E, et al. (2014) Mutations in SLC13A5 cause autosomal-recessive epileptic encephalopathy with seizure onset in the first days of life. *Am J Hum Genet* **95**:113–120.
Wang PY, Neretti N, Whitaker R, Hosier S, Chang C, Lu D, Rogina B, and Helfand SL (2009) Long-lived *Indy* and calorie restriction interact to extend life span. *Proc Natl Acad Sci USA* **106**:9262–9267.
Weerachayaphorn J and Pajor AM (2007) Sodium-dependent extracellular accessibility of Lys-84 in the sodium/dicarboxylate cotransporter. *J Biol Chem* **282**:20213–20220.

Address correspondence to: Dr. Ana M. Pajor, University of California San Diego, Skaggs School of Pharmacy and Pharmaceutical Sciences, 9500 Gilman Dr., La Jolla, CA 92093-0714. E-mail: apajor@ucsd.edu

Molecular Pharmacology

Supplemental Information, Figures and Tables for:

MOL #105049

Molecular basis for inhibition of the Na^+/citrate transporter, NaCT (SLC13A5) by dicarboxylate inhibitors.

Ana M. Pajor, Cesar A. de Oliveira, Kun Song, Kim Huard, Veerabahu Shanmugasundraram, Derek M. Erion.

Supplemental Table 1. Citrate kinetics in wild-type and mutant NaCT. Wild-type and mutant NaCT were expressed in HEK-293 cells in 96 well plates. Transport of ^{14}C-citrate was measured for 30 minutes in sodium containing buffer. Data shown are mean and standard error (n=3) or ½ range (n=2).

Mutant	Km (μM)	Vmax (pmol/min-well)	n
NaCT wild type	330 ± 46	32 ± 6	3
Q77K	343 ± 129	21 ± 3	2
T86Y	367 ± 41	17 ± 2	3
G228A	3978 ± 658	33 ± 4	2
V231A	141 ± 1	15 ± 3	2
V231L	384 ± 117	28 ± 5	2
V232A	1208 ± 446	19 ± 1	2
G409N	4318 ± 916	34 ± 2	2

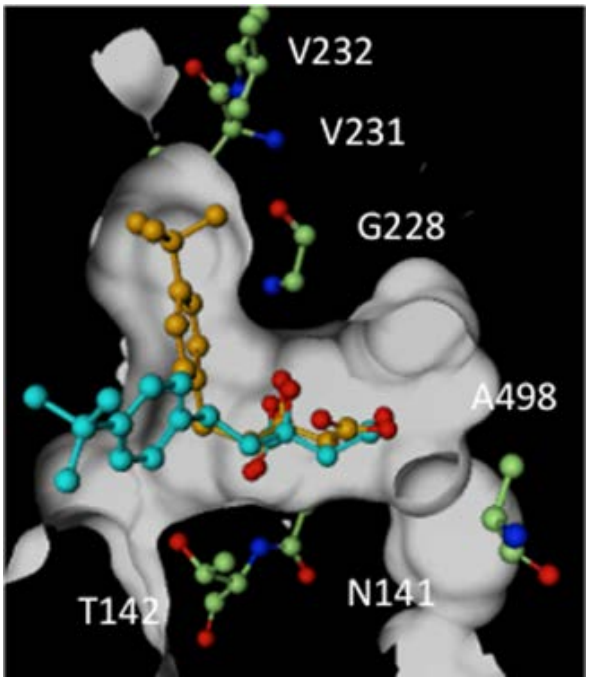

Supplemental Figure 1 Model of the NaCT binding site showing the two most optimal docking poses for compound **2,** in cyan and orange. The docking score (GlideXP) for the orange pose was calculated to be -9.15 and the cyan pose was -8.60. This is a significant difference and thus the orange binding mode was proposed as the preferred binding orientation. This pose presents the t-butyl phenyl group in an orientation that is directly interacting and in the vicinity of residues located at the helices connecting each side of the transporter.

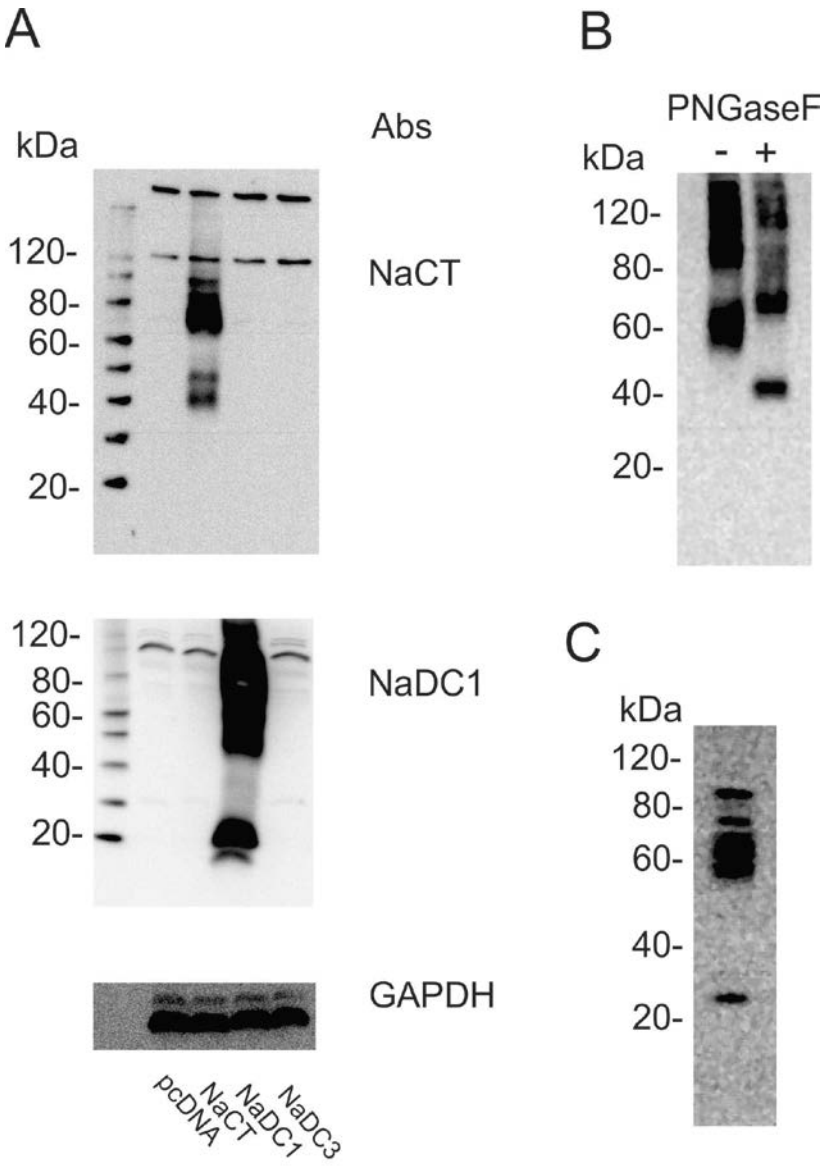

Supplemental Figure 2. Western blots for anti-NaCT antibody characterization. **A**. Specificity of anti-NaCT antibodies. Western blots with total protein lysates from HEK-293 cells transfected with pcDNA (empty vector), or hNaCT, hNaDC1, hNaDC3 in pcDNA. The upper blot was probed with anti-NaCT antibodies (dilution 1:750) which recognize only NaCT. The middle blot was probed with anti-NaDC1 antibodies described in previous studies (Pajor and Sun, 2010; Pajor et al., 1998), which are specific for NaDC1. The lower blot was probed with GAPDH to show sample loading. **B.** The multiple protein bands recognized by anti-NaCT antibodies are differently glycosylated forms of the protein. Cell lysates (as in A) were incubated with (+) or without (-) PNGase F (Pajor and Sun, 2010). **C.** Western blot of human liver S9 fraction probed with the anti-NaCT antibodies. Size standards (Magic Mark XP, ThermoFisher) are indicated on each blot.

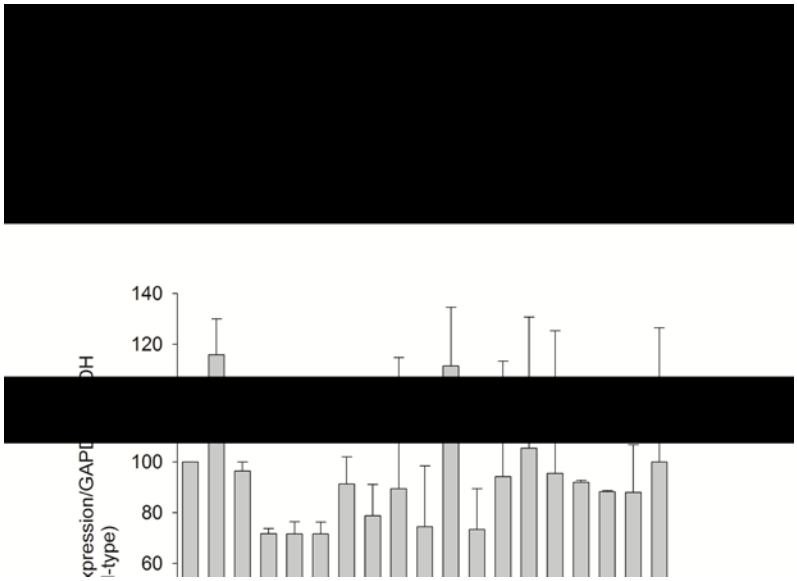

Supplemental Figure 3. Protein expression of NaCT mutants normalized to GAPDH. Western blots (as in Figure 6A) of whole cell lysates from wild-type and mutant NaCT were probed with anti-NaCT and anti-GAPDH antibodies. The signal was quantitated and expressed as a ratio of NaCT/GAPDH. The ratio for each mutant was then normalized to the ratio for wild-type in the same blot. Each bar represents the mean and range of 2 independent experiments.

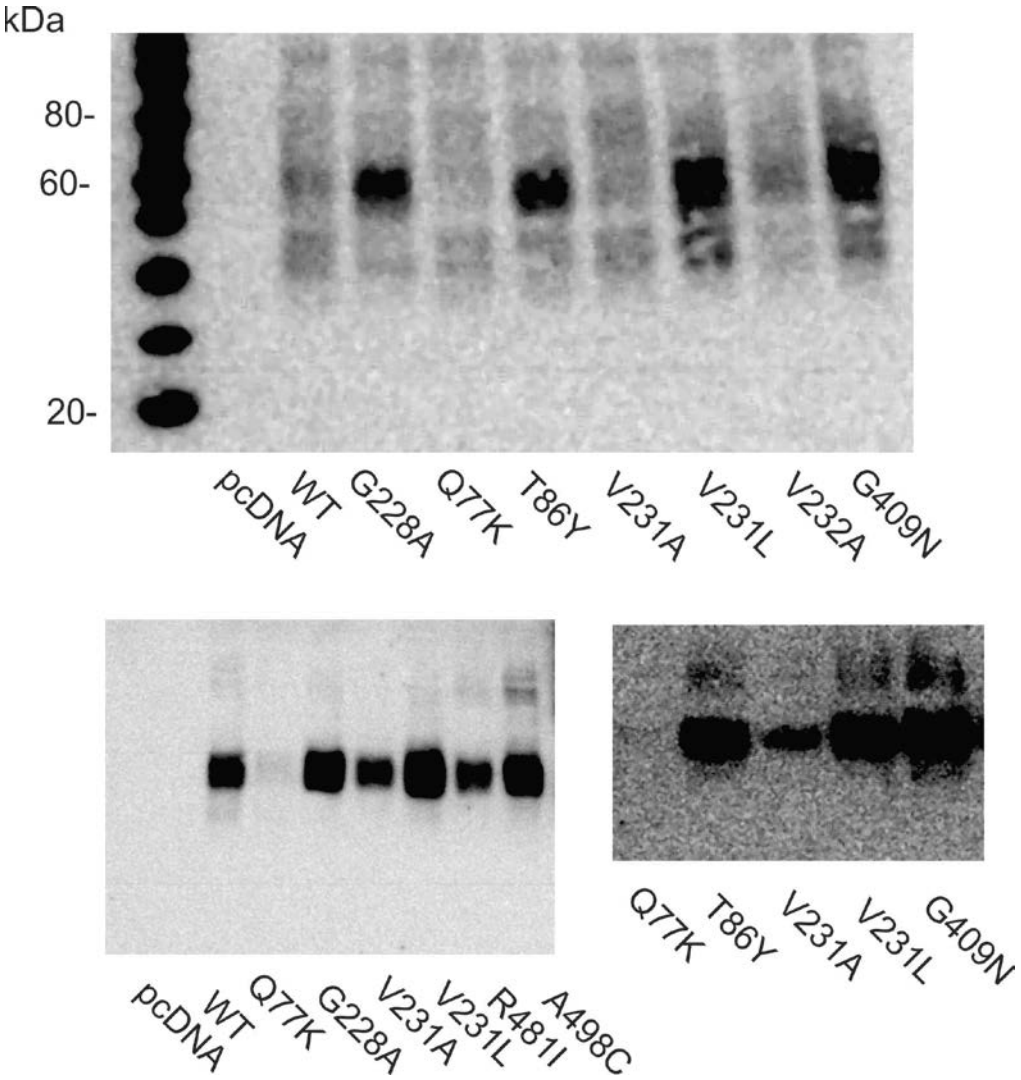

Supplemental Figure 4. Cell surface biotinylations of wild-type (WT) NaCT and mutants. Cell monolayers were treated with Sulfo-NHS-LC-biotin as in Fig. 6B. The Western blots were probed with anti-NaCT antibodies. The figure has three separate blots with samples from different passage numbers and transfection dates, and shows the variability in signal between experiments.

Supplemental Table 2 IC_{50} values for compound 2 and compound 4 from curves such as Figure 8B and Figure 9B. HEK-293 cells were transfected with plasmids expressing wild type or mutant NaCT and ^{14}C-citrate transport was measured at increasing concentrations of inhibitors. The mean and SEM from three independent experiments, with cells from different passage numbers, are shown. Sample size is (N). CF, the data could not be fitted accurately. * denotes $P < 0.05$ compared with wild-type.

Mutant	**Compound 2** **IC_{50} (μM) (N)**	**Compound 4** **IC_{50} (μM) (N)**
NaCT (wild type)	0.9 ± 0.2 (3)	1.4 ± 0.1 (3)
Q77K	0.5 ± 0.1 (3)	0.4 ± 0.2 (3)*
T86Y	0.1 ± 0.02 (3) *	0.1 ± 0.04 (3)*
G228A	CF, CF (2)	CF, CF (2)
V231A	0.1 ± 0 (3) *	0.1 ± 0.05 (3)*
V231L	CF, CF, CF (3)	0.5 ± 0.1 (3)*
V232A	30, 24, CF (3)	1, 0.5, CF (3)
G409N	CF, CF (2)	CF, CF, CF (3)

Supplemental Table 3. Results from IC_{50} experiments with G228A and G409N mutants. Citrate transport activity remaining after incubation with 25 or 250 μM compound 2 or 25 μM compound 4, shown as a percentage of control incubated with DMSO only. The results are from two or three independent experiments.

Mutant	**Compound 2** **Citrate transport (% control)**		**Compound 4** **Citrate transport (% control)**
	25 μM	**250 μM**	**25 μM**
G228A	75, 69	55, 60	41, 77
G409N	60, 64	50, 56	56, 65, 89

Reference List

Pajor AM, Sun N and Valmonte H G (1998) Mutational Analysis of Histidines in the Na^+/Dicarboxylate Cotransporter, NaDC-1. *Biochem J* **331**:257-264.

Pajor AM and Sun N N (2010) Single Nucleotide Polymorphisms in the Human Na^+-Dicarboxylate Cotransporter Affect Transport Activity and Protein Expression. *Am J Physiol Renal Physiol* **299**:F704-F711.